



Adsorption of paraquat on mesoporous silica modified with titania: Effects of pH, ionic strength and temperature

Maximiliano Brigante*, Pablo C. Schulz

INQUISUR, Departamento de Química, Universidad Nacional del Sur, Av. Alem 1253, 8000 Bahía Blanca, Argentina

ARTICLE INFO

Article history:

Received 28 May 2011

Accepted 15 July 2011

Available online 27 July 2011

Keywords:

Paraquat

Silica

Titania

Solid–water interface

Adsorption

Surface complexes

ABSTRACT

The adsorption of the herbicide paraquat (PQ^{2+}) on the binary system titania–silica has been studied in batch experiments by performing adsorption isotherms under different conditions of pH, supporting electrolyte concentration, and temperature. Adsorption kinetic on the studied material has also been carried out and discussed. PQ^{2+} adsorption is very low on the bare silica surface but important on the composed TiO_2 – SiO_2 adsorbent. In this last case, the adsorption increases by increasing pH and decreasing electrolyte concentration. There are no significant effects of temperature on the adsorption. The increase of the adsorption in TiO_2 – SiO_2 seems to be related to an increase in acid sites of the supported titania and to the homogenously dispersion of the TiO_2 nanoparticles over the silica support. The adsorption takes place by direct binding of PQ^{2+} to TiO_2 leading to the formation of surface species of the type SiO_2 – TiO_2 – PQ^{2+} . Electrostatic interactions and charge-transfer and outer-sphere complexes formations seem to play a key role in the adsorption mechanism. The analysis of thermodynamic parameters suggests that the adsorption on TiO_2 – SiO_2 is endothermic and spontaneous in nature.

© 2011 Elsevier Inc. All rights reserved.

1. Introduction

A major environmental concern at present is the contamination of aquatic systems due to pesticide discharges from manufacturing plants, surface runoff, leaching accidental spills and other sources [1]. Among the numerous agrochemicals in use today, the herbicide paraquat (1,1'-dimethyl-4,4'-dipyridinium chloride) is widely used in a variety of applications owing to its physical and chemical properties, such as high solubility in water, low vapor pressure and high binding potential, which makes it suitable for many agriculture uses [2]. However, it is known that this herbicide is one of the most toxic poisons if deliberately or accidentally ingested [3]. In recent years, investigations on paraquat toxicity have suggested that this herbicide might be an environmental factor contributing to a neurodegenerative disorder, such as Parkinson's disease [4]. Paraquat (PQ^{2+}), also known under the name of methyl viologen, is frequently used as an efficient electron transfer-reagent in electrochemistry and bioelectrochemistry [5]. It is easily reduced to stable, highly colored PQ^{+} radical. The herbicidal activity is, in effect, also a consequence of the formation of PQ^{+} radicals.

Adsorption from aqueous solutions to solid surfaces is one of the key processes determining the concentration and rate of transport of herbicides in the environment and it is important from the point of view of inhibiting herbicides toxic properties into water systems [6–8]. However, it is known that the adsorption of PQ^{2+}

vary largely with the nature of the adsorbent. PQ^{2+} adsorbs strongly on clay minerals, somewhat less on activated carbon and humic substances, and negligible on iron oxides [9–12]. For this reason, researchers have focused their attention on the synthesis of new materials for pollutant remotion, mainly on solids with high surface area, pore size and catalytic activity.

Since 1990, mesoporous silica and silica-based materials have attracted considerable attention because of their high surface area ($>200 \text{ m}^2 \text{ g}^{-1}$), ordered frameworks, narrow pore size distribution ($2 > 10 \text{ nm}$, higher than zeolites) and high thermal stability [13–15]. Due to these properties, they are ideal base materials for catalyst, catalyst support and adsorbent as well as template for other materials. However, pure silica shows limited applications because the neutral frame-structure of this material leads to a lack of acid sites and acidity [16], that significantly lowers the cation-exchange capacities and reactivity [17]. A solution to this problem is the incorporation of active metals and/or metal oxides into the mesopore structure [18]. One of the widely used oxides in this sense is titanium dioxide or titania due to its high photocatalytic activity, low cost, non-toxicity and high stability in aqueous solution [19–21].

The aim of this article is to present a study of PQ^{2+} adsorption on titania-modified silica (TiO_2 – SiO_2). The data obtained at a variety of pH, ionic strength and temperature are used to gain insights into the mechanisms that govern the adsorption process and into the factors that promote or prevent adsorption. The obtained results will also serve as a basis for further synthesis of new materials for pollution control.

* Corresponding author.

E-mail address: brigante@uns.edu.ar (M. Brigante).

2. Materials and methods

2.1. Chemicals

Paraquat dichloride (MW = 257.16 g mol⁻¹), sodium dioctyl sulfosuccinate (Aerosol OT, AOT) 99%, tetraethyl orthosilicate (TEOS, 99%), hexadecyl (=cetyl) trimethylammonium bromide (CTAB) were obtained from Sigma–Aldrich. TiCl₄ (99%, $\delta = 1.722$ g cm⁻³) and *n*-hexane were purchased from Carlo Erba. NaOH, sodium acetate, acetic acid, sodium carbonate, sodium hydrogen carbonate, disodium phosphate anhydrous and monosodium phosphate anhydrous were obtained from Anedra. All chemicals were of analytical grade and used as received. Doubly distilled water was used for the preparation of solutions for experiments.

2.2. SiO₂ and SiO₂–TiO₂ materials. Synthesis and general characterization

Synthesis of SiO₂ and composed TiO₂–SiO₂ materials were carried out using a procedure similar to that described by Messina et al. [22]. To obtain the mesoporous silica, 11.6 mL of TEOS were mixed with 2 mL of water and stirred for 10 min at 500 rpm. Then, a solution formed by 1.1 g of NaOH in 20 mL of water was added drop to drop to the TEOS solution under stirring. To produce a SiO₂ material, a solution of 7.62 g of CTAB in 38 mL of water was added 1 min after the addition of the NaOH solution. The resulting gel was stirred for 3 min and then left for 48 h in an autoclave at 100 °C. Then, the gel was filtered and washed with distilled water and left to dry at room temperature. Finally, it was calcined by increasing the temperature from room temperature to 540 °C with a heating rate of 2 °C min⁻¹, and holding for 7 h at 540 °C in an air flux.

TiO₂ was obtained by using an inverse microemulsion composed by *n*-hexane/water/Aerosol OT (AOT). The water microdroplets surrounded by a monolayer of surfactant in a continuous hydrocarbon phase act as micro-reactors to synthesize nanoparticles whose growth is controlled inside the water droplet giving rise to a narrow size distribution [22]. The AOT microemulsion was prepared with a water/surfactant ratio $W = 10$. In a flask, 1.1276 g AOT and 0.46 g water were weighed, and then the sample was left during 3 h to produce the surfactant hydration. Then, 80 mL of *n*-hexane were added and the system sonicated to produce the microemulsion. Then, 1.4 mL of TiCl₄ were added and left 3 days to react following the reaction:



To obtain the TiO₂ nanoparticles, the HCl and *n*-hexane were eliminated by evaporation under vacuum. A white compound formed by the titania nanoparticles surrounded by AOT was obtained. Then, the material was calcined during 7 h at 540 °C with air flux.

TiO₂–SiO₂ was prepared by addition of 2.8 g of the dry AOT–TiO₂ material obtained without calcination to the solution of CTAB in water and then sonicated to complete suspension of the material. The resulting solution was added to the TEOS + NaOH solution, and the system was treated as that without TiO₂. The TiO₂ content on the silica support was 28 wt.%, which was confirmed by XRD and SEM-EDX (see below).

The synthesized materials were characterized by the techniques usually employed in porous materials, such as scanning and transmission electron microscopy; X-ray diffraction (XRD); FT-IR; electrophoretic mobility measurements; and the N₂–BET method for surface area, pore volume and pore diameter determination. Scanning electron microscopy (SEM) was performed using a LEO 40-XVP microscope equipped with a secondary electrons detector

and an X-ray microanalysis system (EDAX DX-4). The samples were prepared on graphite stubs and coated with a ca. 300 Å gold layer in a PELCO 91000 sputter coater. Transmission electron microscopy (TEM) was performed using a JEOL 100 CX II transmission electron microscope, operated at 100 kV with magnification from 50,000× to 200,000×. Observations were made in a bright field. Powdered samples were placed on cooper supports of 2000 mesh. XRD patterns were collected via a Philips PW 1710 diffractometer with Cu K α radiation ($\lambda = 1.5406$ Å) and graphite monochromator operated at 45 kV, 30 mA and 25 °C. The zeta potentials and the isoelectric point (IEP) of the samples were measured with a Zetasizer Nano Series instrument (Malvern Instruments Ltd.) at room temperature. Stock SiO₂, TiO₂, and TiO₂–SiO₂ suspensions containing 0.1 g L⁻¹ of solid in 10⁻² M KNO₃ were used for those purposes. The pH of the suspensions was then adjusted to the desired value by adding small volumes of HNO₃ or KOH solutions. The N₂ adsorption isotherms at 77.6 K were measured with a Micrometrics Model Accelerated Surface Area and Porosimetry System (ASAP) 2020 instrument. Each sample was degassed at 373 K for 720 min at a pressure of 10⁻⁴ Pa. FT-IR experiments were recorded in a Nicolet FT-IR Nexus 470 Spectrophotometer. To avoid co-adsorbed water, the samples were dried under vacuum until constant weight was achieved and diluted with KBr powder before the FT-IR spectra were recorded.

2.3. Adsorption experiments

Adsorption experiments were obtained with a batch equilibration procedure using 15-mL polypropylene centrifuge tubes covered with polypropylene caps immersed in a thermostatic shaker bath. Before starting the experiment, a stock PQ²⁺ solution (1 × 10⁻³ M) was prepared by adding the corresponding solid to pH buffer solutions. The pHs used in these studies were 4.4, 7.0 and 9.5 by using 0.1 M acetate/acetic acid, HPO₄⁻²/H₂PO₄⁻¹ and CO₃⁻²/HCO₃⁻¹ buffer solutions, respectively. Fifty milligrams of adsorbent was introduced into the tubes and mixed with varying quantities of PQ²⁺ and KCl (used as supporting electrolyte) solutions. The range of initial PQ²⁺ concentration was 4–500 μM, and the final volume was 8 mL. The mixture was stirred for 4 h at 90 rpm and centrifuged to separate the phases. An aliquot of the supernatant was analyzed to quantify the PQ²⁺ remaining in the supernatant and to calculate the adsorbed amount of PQ²⁺. In most experiments, no supporting electrolyte was used and the working temperature was 25 °C (except when effects of ionic strength and temperature were investigated). For the batch kinetic studies, the initial PQ²⁺ concentration was 5 × 10⁻⁴ M. The mixtures were shaken for different reaction times in order to achieve complete adsorption or to gather enough data points.

Quantification of PQ²⁺ was performed by UV–vis spectroscopy at 258 nm using an Agilent 8453 UV–vis diode array spectrophotometer equipped with a Hellma 1-cm quartz cell. The supernatant of the withdrawn aliquot was placed into the cell and the spectrum was recorded in the 200–900 nm wavelength range. Calibration curves at the working pH were also constructed with several PQ²⁺ solutions having concentration that ranged between 2 and 150 μM. Very good linearity was found in all cases.

The adsorption isotherms were fitted using the Freundlich equation, which was commonly used in the adsorption of herbicides on several adsorbent systems [23,24]. The linear form of this equation is displayed as follow:

$$\ln \text{PQ}_{\text{ads}}^{2+} = \ln K_F + \frac{1}{n} \ln \text{PQ}_{\text{eq}}^{2+} \quad (2)$$

where PQ_{ads}²⁺ is the adsorbed amount of PQ²⁺ (μmol g⁻¹), PQ_{eq}²⁺ is the equilibrium concentration of PQ²⁺ in the supernatant (μM), K_F is the

Freundlich constant (μM^{-1}), and $1/n$ is the adsorption intensity. PQ_{ads}^{2+} was calculated with the equation

$$PQ_{\text{ads}}^{2+} = \frac{(PQ_0^{2+} - PQ_{\text{eq}}^{2+})V}{m}, \quad (3)$$

where PQ_0^{2+} is the initial concentration of the antibiotic (μM), V the solution volume (L) and m is the adsorbent mass (g). From the linearized form of Eq. (2) K_F , $1/n$ and the correlation coefficient, r^2 can be calculated.

3. Results and discussion

3.1. General characteristics of the synthesized materials

Fig. 1 shows the X-ray diffractograms of SiO_2 , TiO_2 (after calcination) and $\text{TiO}_2\text{-SiO}_2$ materials. SiO_2 shows a typical amorphous XRD patterns which is characteristic of mesoporous silicas [25]. This means that the mesoporous structure of SiO_2 is stable under our synthesis conditions and it does not collapse during calcination at 540°C resulting in transformation to the cristobalite phase [26].

Titania shows several diffraction peaks, relating to the formation of a mixed phase composed by anatase ($2\theta = 25.32^\circ$, 37.85° , 48.09° , and 53.93°) and rutile ($2\theta = 27.48^\circ$, 36.10° , 54.36° , and 56.68°) [27] in a 5:1 M ratio. However, the rutile diffraction peaks disappear in the XRD patterns of $\text{TiO}_2\text{-SiO}_2$ evidencing that anatase is the only titania crystalline phase. The rutile phase is essentially formed at higher calcination temperatures ($>723\text{ K}$ or above) [28]. However, the nonappearance of rutile diffraction peaks in $\text{TiO}_2\text{-SiO}_2$ is in agreement with Yang et al. [29], who reported that silica plays a key role in the inhibition of the formation of rutile phase. It is also interesting to note that supported TiO_2 shows broad diffraction peaks in comparison to free titania, suggesting the formation of dispersed TiO_2 nanocrystallites [30]. In fact, the grain sizes of free and supported TiO_2 , determined from the width at half maximum of the anatase (1 0 1) peak according to the Scherrer formula [31], are 13 and 4 nm, respectively. These values of grain size are consistent with the TEM studies.

The morphology of the studied samples was also investigated by SEM and TEM techniques and the respective micrographs are presented in Fig. 2. Bare silica (Fig. 2a) shows randomly shaped aggregates of variable size and these do not provide a clear morphology. TEM image (Fig. 2b) seems to show a typical hexagonal arrangement of mesopores whose dimensions may be engineered in the range of $\sim 18\text{ nm}$. TiO_2 particles also show randomly shaped aggregates probably due to a faster condensation of titania (Fig. 2c). The aggregates are formed by nanoparticles whose average diameter was 15 nm. The structure of the particles seems to be

tetrahedral instead of rhombic (Fig. 2d). This means that the structure of particles is that of rutile or anatase, not that of brookite. The morphology of TiO_2 loaded on the silica material (Fig. 2e) is similar to that of silica support and does not show clearly titania crystallites. This may indicate the formation of fine particles and dispersion of TiO_2 over the support or into the mesopores [25]. From the TEM images, it appears that TiO_2 nanoparticles (black spot) are distributed in both the pores and the pore walls (Fig. 2f). The diameter of titania nanoparticles on the mesopores structure is around 5–7 nm, which is smaller than titania particles obtained by calcination. This may mean that calcination produces synerization of the particles, while the presence of the silica structures allows separation of the original particles and avoids the synerization [22].

The nitrogen adsorption–desorption isotherms of the studied materials are shown in Fig. 3.

The adsorption/desorption isotherm on TiO_2 (i) is type II [32]. It represents unrestricted monolayer–multilayer adsorption. There is a hysteresis of type H4, which is associated with narrow slit-like pores. Similar results were reported by Zubietta et al. in porous TiO_2 and $\text{TiO}_2\text{-chitosan}$ materials [33]. In the case of slit-like pores, the determined diameter is the pore width. However, SiO_2 (ii) and $\text{TiO}_2\text{-SiO}_2$ (iii) represent typical type IV isotherms with a H2 hysteresis loop that is characteristic of mesopores [22]. Specific surface area, pore diameter and pore volume of the solids are summarized in Table 1. It may be seen that in general, the specific areas of the materials here synthesized are low. In literature, there are examples of mesoporous materials made with silica including other oxides which have poor specific surface areas, and these areas depend on the synthesis conditions [34]. The average pore diameter of SiO_2 was around 18 nm, which is in agreement to those reported in TEM microscopy. Table 1 also shows that $\text{TiO}_2\text{-SiO}_2$ has higher surface area and lower pore diameter than bare SiO_2 . On the one hand, the increase in A_{BET} is attributed to the start growing of the TiO_2 crystallites on the outer surface of SiO_2 [35]. On the other hand, the decrease pore size is attributed to the presence of TiO_2 dispersed into the mesopores [36].

FT-IR spectra of SiO_2 , TiO_2 and $\text{TiO}_2\text{-SiO}_2$ are shown in Fig. 4. The most important features of SiO_2 are a broad band centered at 3625 cm^{-1} associated to OH stretch from surface hydroxyls bound to silica (Si–OH); a broad peak located at 1091 cm^{-1} which is attributed to asymmetric Si–O–Si vibrations; two peaks centered at 797 and 622 cm^{-1} due to symmetric Si–O–Si vibrations; and a peak at 478 cm^{-1} assigned for Si–O–Si bending modes [37]. TiO_2 shows characteristic absorption bands at around 3478 , 1633 (shoulder), 1123 , and 486 cm^{-1} which are attributed to O–H stretching vibration of the adsorbed water and hydroxyl groups on the surface, O–H bending, Ti–O stretching and Ti–O–Ti vibrations, respectively [27].

Some differences can be observed in the FT-IR spectra of $\text{TiO}_2\text{-SiO}_2$ material. One such difference is the decrease in the intensity of the 797 and 622 cm^{-1} peaks (the last peak decreases up to disappear), corresponding to the symmetric Si–O–Si vibrations. In addition, the band situated at 1091 cm^{-1} corresponding to asymmetric Si–O–Si vibrations is shifted toward lower wavenumber with decrease in broadness. Several works have described a new peak located at 960 cm^{-1} which is attributed to Ti–O–Si vibrations [37,38]. This peak appears in our spectra as a shoulder in the broad peak located at around 1110 cm^{-1} . These changes in the FT-IR spectra are significant evidences that TiO_2 interacts with the silica support through chemical bonding, similar as those reported in several reviews [39,40].

Fig. 5 shows the electrophoretic mobility data at different values of pH for the studied materials.

The IEPs of bare silica and titania are 3.5 and 6.7 pH units, which are in agreement with those reported in literature [41]. The IEP of

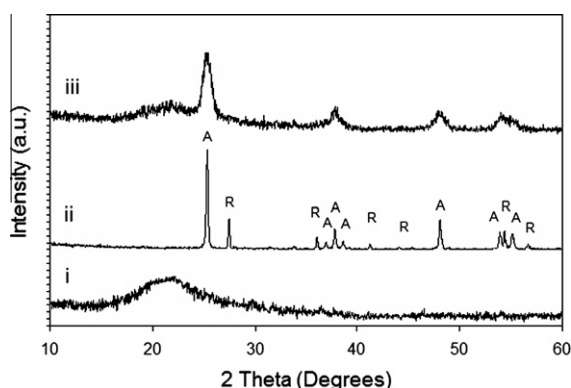


Fig. 1. XRD patterns of the synthesized: (i) SiO_2 , (ii) TiO_2 and (iii) $\text{TiO}_2\text{-SiO}_2$. A = anatase, R = rutile.

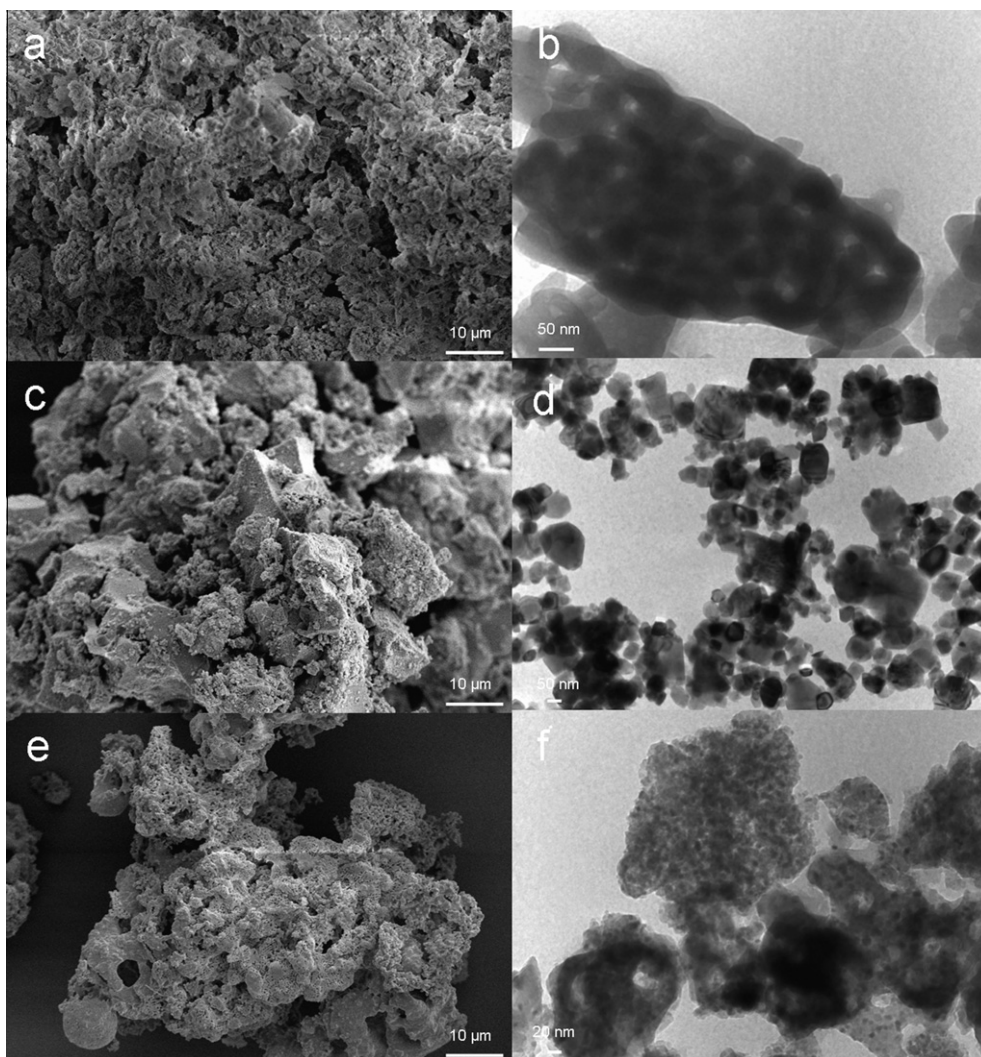


Fig. 2. SEM (left side) and TEM (right side) micrographs of (a and b) SiO_2 , (c and d) TiO_2 and (e and f) $\text{TiO}_2\text{-SiO}_2$.

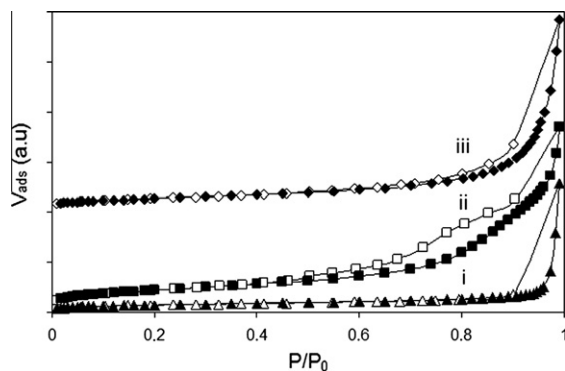


Fig. 3. Nitrogen adsorption (open symbols)–desorption (solid symbols) isotherms on (i) TiO_2 , (ii) SiO_2 and (iii) $\text{TiO}_2\text{-SiO}_2$.

$\text{TiO}_2\text{-SiO}_2$ shifts to lower pH in comparison to TiO_2 , which indicates an increase in acidity of titania surface. There are several reports that supports the hypothesis that silica induces an increase in acidity (or negative sites) to TiO_2 at high Si:Ti molar ratio [42–44]. On the contrary, Lee et al. [45] show that the IEP of the $\text{TiO}_2\text{-SiO}_2$ shifts to IEP of bare titania as TiO_2 content increases suggesting that titania encapsulates to SiO_2 particles. From TEM images (see

Table 1

Nitrogen adsorption results on the studied solids.

Sample	A_{BET} ($\text{m}^2 \text{g}^{-1}$)	D_{aap} (nm)	V_{spat} ($\text{cm}^3 \text{g}^{-1}$)
SiO_2	238.6	18.89	0.4104
28 wt.% $\text{TiO}_2\text{-SiO}_2$	259.2	7.77	0.4003
TiO_2	9.5	21.09	0.0499

Note: A_{BET} : BET surface area; D_{aap} : adsorption average pore diameter by BET (8 V/A); V_{spat} : single point adsorption total pore volume of pores.

Fig. 2f), it can be seen that the complete encapsulation of SiO_2 by TiO_2 is not detected in our binary system which is consistent with $\text{IEP}_{\text{TiO}_2\text{-SiO}_2} < \text{IEP}_{\text{TiO}_2}$.

3.2. PQ^{2+} adsorption studies

The adsorption of PQ^{2+} on $\text{TiO}_2\text{-SiO}_2$ at pH 9.5 as a function of time was shown in Fig. 6.

The adsorption is very fast between $t = 0$ and 5 min. It is so fast that no data point could be measured in this period with our experimental set up. At $t > 5$ min, the adsorption takes place at a much slower and measurable rate. The equilibrium was reached after 60 min of reaction. The data were fitted well to the pseudo-second-order kinetic model with $r^2 = 0.9998$. The initial rate and

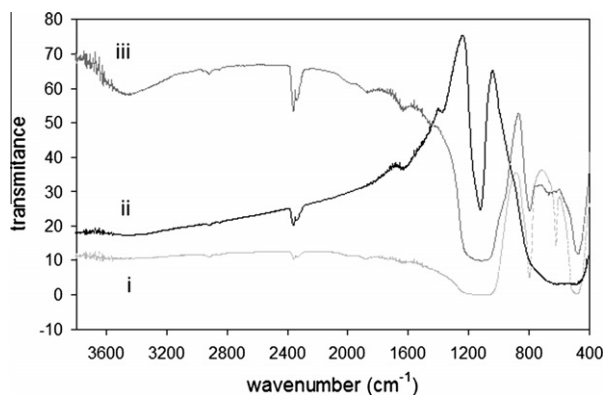


Fig. 4. Infrared spectra of (i) SiO₂, (ii) TiO₂, and (iii) TiO₂-SiO₂.

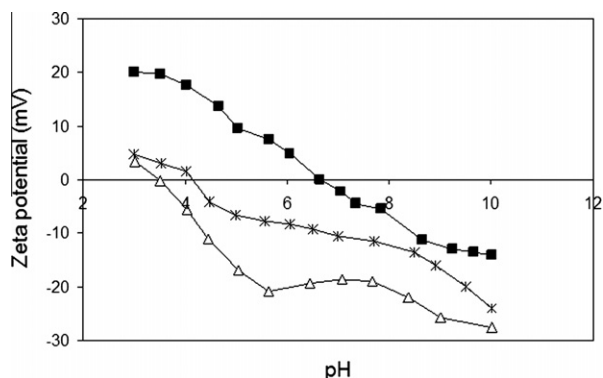


Fig. 5. Electrophoretic mobilities of the studied samples as a function of pH in 10^{-3} M KNO₃ solution: solid squares, TiO₂; stars, TiO₂-SiO₂; and open triangles, SiO₂.

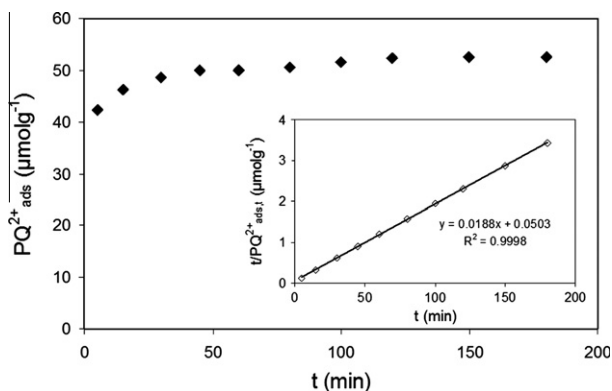


Fig. 6. Adsorption kinetics of PQ²⁺ on TiO₂-SiO₂ at pH 9.5 and 25 °C. The insert is the linear plot of the pseudo-second-order fit.

the amount of PQ²⁺ adsorbed in the equilibrium were $7.03 \times 10^{-3} \mu\text{mol g}^{-1} \text{ min}^{-1}$ ($0.027 \text{ g mg}^{-1} \text{ min}^{-1}$) and $53.19 \mu\text{mol g}^{-1}$ (13.68 mg g^{-1}), respectively. These values are comparable to those reported by Tsai and co-workers on the adsorption of PQ²⁺ on diatomite and activated bleaching earth at alkaline pH [9,46]. Such results indicate that TiO₂-SiO₂ can act as a good adsorbent for PQ²⁺ kinetically. Although equilibrium could be established quickly, subsequent experiments were equilibrated for 4 h.

Fig. 7 shows the effects of pH on the adsorption isotherms of PQ²⁺ on TiO₂-SiO₂ at 25 °C. Adsorption of the herbicide on silica (open diamonds in Fig. 7) was low and only detectable at pH 9.5. The low adsorption capacity of SiO₂ is attributed to the neutral

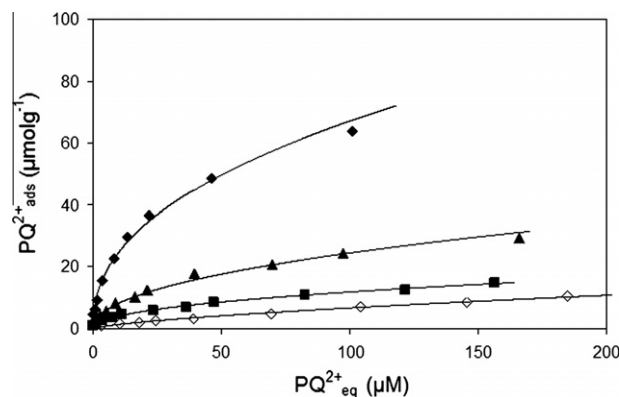


Fig. 7. Effect of pH on the adsorption of PQ²⁺ on SiO₂ (open symbols) and TiO₂-SiO₂ (solid symbols) at 25 °C. Diamonds, pH 9.5; triangles, pH 7; and squares, pH 4.4. Lines show predictions of Eq. (2) with parameters from Table 2.

frame-structure of this material leading to a lack of acid sites and acidity [16]. Preliminary studies also showed that the adsorption of PQ²⁺ on non-supported TiO₂ was negligible in all experimental conditions (pH range between 4.4 and 9.5, data not shown) mainly due to its low surface area.

On the contrary to the adsorption on silica and titania, PQ²⁺ adsorption readily takes place on TiO₂-SiO₂, showing that the presence of TiO₂ favorably affects this process. The shape of the isotherms is similar to the shape of the isotherms reported by Rytwo et al. [47], Iglesias et al. [11] and Burns et al. [48] for the adsorption of PQ²⁺ on negatively charged clays, HA and Ca-humate respectively. Fig. 7 also shows that the adsorption on TiO₂-SiO₂ is strongly dependent on the pH. It is relatively high at high pH and decreases significantly at lower pH values.

PQ²⁺ adsorption on TiO₂-SiO₂ could take place either by direct binding to the SiO₂ or by direct binding to the supported titania surface. The first case does not appear to be important under our experimental conditions since it was shown that attachment to the silica surface was too low. The second case seems to be the most probable. On the one hand, the formation of TiO₂ nanoparticles dispersed on the SiO₂ support offers more active sites for adsorption occur than non-supported TiO₂ (agglomeration of particles) [25]. In addition, the increase in surface acidity (negative sites) of titania due to SiO₂ may enhance its interaction with several cationic species that include PQ²⁺ ions. The increase in surface acidity on supported titania is also reported by Prada Silvy et al. [49] for the TiO₂-Al₂O₃ catalyst. On the other hand, Messina and Schulz [50] reported an increase in adsorption of cationic dyes in the TiO₂-SiO₂ system in comparison to bare silica. The authors attributed this increase to a UV photoinduction from supported TiO₂ catalyst to the dye molecule provoking its degradation. However, this effect was not showed in this work, i.e., PQ²⁺ photodegradation was not detected in adsorption experiments under UV lamp in all experimental conditions (data not shown). The direct binding between PQ²⁺ and supported TiO₂ generates ternary surface species SiO₂-TiO₂-PQ²⁺, whose formation is mainly driven by PQ²⁺-TiO₂ electrostatic interactions, where negatively charged groups of titania could bind the dication by forming ionic pairs or outer-sphere complexes. The increase in adsorption by increasing pH will increase the degree of dissociation of TiO₂ functional groups, leading to an increased electrostatic attraction between PQ²⁺ and TiO₂-SiO₂ and a higher adsorption.

The effects of ionic strength on the adsorption of PQ²⁺ isotherms on TiO₂-SiO₂ at pH 9.5 and 25 °C are shown in Fig. 8. The adsorption depends on the ionic strength; it decreases as the KCl concentration increases. These results suggest that formation of ionic pairs or outer-sphere complexes is the prevailing adsorption

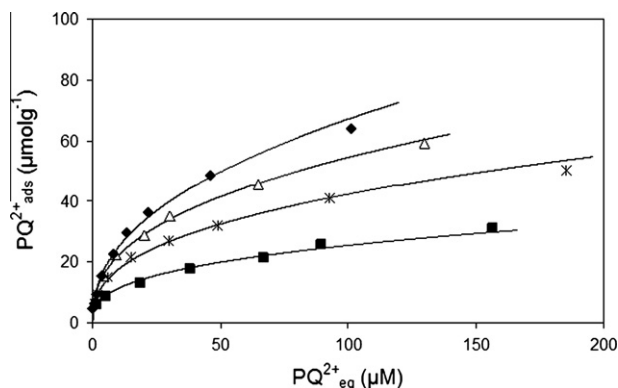


Fig. 8. Effect of ionic strength on the adsorption of PQ^{2+} on TiO_2-SiO_2 at pH 9.5 and 25 °C. KCl concentrations: solid diamonds, 0 M; open triangles, 0.01 M; stars, 0.03 M; and solid squares, 0.1 M. Lines show predictions of Eq. (2) with parameters from Table 2.

process: the competition between PQ^{2+} and K^+ for negatively charge groups leads to an important decrease in PQ^{2+} adsorption by increasing K^+ concentration. The results resemble those reported by Tsai et al. [46] for the adsorption of PQ^{2+} on activated clays, where competition between PQ^{2+} and electrolyte cations was proposed to play a key role.

The effects of temperature on the adsorption of PQ^{2+} isotherms on TiO_2-SiO_2 at pH 9.5 are shown in Fig. 9. PQ^{2+} adsorption is not significantly affected by varying the temperature from 5 to 45 °C, i.e., the adsorption slightly increases as temperature increases. The maximum uptake was between 63 and 67 $\mu\text{mol g}^{-1}$ at all investigated temperatures.

Several reports exist about the effect of temperature in the adsorption behavior of PQ^{2+} on different adsorbents. Tsai and Lai [9] showed that the adsorption of PQ^{2+} on clay minerals strongly increased by increasing temperature suggesting that a chemisorption-like process may play an important role in the PQ^{2+} -clay adsorbent system. These observations are significantly different from those reported by Nakamura et al. [10], who reported that PQ^{2+} adsorption on activated carbon decreased by increasing temperature (physical adsorption). None of these mechanisms are in agreement with data shown in Fig. 9, indicating that temperature effects on PQ^{2+} adsorption are strongly dependent on the type of adsorbent. The no strong dependence of the adsorption of PQ^{2+} with the temperature is consistent with formation of ionic pairs or outer-sphere complexes, where there is competition with the cations of the supporting electrolyte. If changes in temperature affect in a similar way the affinity of PQ^{2+} and K^+ for negatively

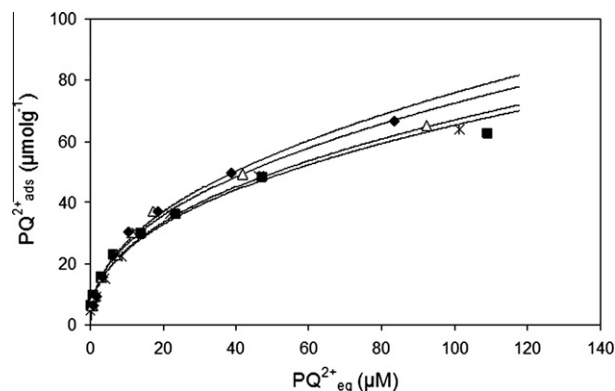


Fig. 9. Effect of temperature on the adsorption of PQ^{2+} on TiO_2-SiO_2 at pH 9.5. Solid diamonds, 45 °C; open triangles, 35 °C; stars, 25 °C; and solid squares, 15 °C. Lines show predictions of Eq. (2) with parameters from Table 2.

charged sites, there will be no significant temperature effects by changing the temperature.

From the data showed in Fig. 9 were obtained the thermodynamic parameters of the Gibbs free energy (ΔG°), enthalpy (ΔH°) and the entropy (ΔS°) for the adsorption of PQ^{2+} on the studied material using the following equations:

$$\Delta G^\circ = RT \ln \left(\frac{PQ_s^{2+}}{PQ_{eq}^{2+}} \right), \quad (4)$$

$$\ln \left(\frac{PQ_s^{2+}}{PQ_{eq}^{2+}} \right) = \frac{\Delta S^\circ}{R} - \frac{\Delta H^\circ}{RT}, \quad (5)$$

where PQ_s^{2+} is the concentration of antibiotic adsorbed (μM), T is the solution temperature in K and R is the gas constant ($8.314 \text{ J K}^{-1} \text{ mol}^{-1}$). The enthalpy of the PQ^{2+} on TiO_2-SiO_2 is obtained from van't Hoff plots as $\ln(PQ_s^{2+}/PQ_{eq}^{2+})$ versus $1/T$. The thermodynamic parameters are shown in Table 2. The ΔH° value for the adsorption of PQ^{2+} on the studied material is positive and 8.45 kJ mol^{-1} implying that the interaction of PQ^{2+} with the solid is an endothermic process. The low ΔH° value is attributed to a number of physical interactions involving electrostatic interactions and formation of outer-sphere complexes between the PQ^{2+} and the adsorbent structure [10,51]. In addition, the positive enthalpy value possibly may imply some structural changes of PQ^{2+} . For example, transformation to highly colored PQ^+ radicals and/or formation of charge-transfer complexes between PQ^{2+} and the negatively charged functional groups of the TiO_2 [5,52,53]. Formation of radical ions was not detected in our results mainly because both the TiO_2-SiO_2 surface and the herbicide supernatant were not colored during the adsorption experiments carried out. The positive value of ΔS° ($39.88 \text{ J K}^{-1} \text{ mol}^{-1}$) reflects the affinity of the herbicide toward the solid and may suggest some structural changes in adsorbate (hydration of PQ^{2+} ions) and adsorbent (charged surface upon adsorption) [54]. Finally, the negative value of ΔG° at various temperatures shows that the nature of adsorption on both adsorbents is spontaneous.

In Figs. 7–9, symbols correspond to data points whereas solid lines correspond to the best-fitting Freundlich isotherms calculated by adjusting the parameters n and K_F . These parameters are listed in Table 3. Even though the formulated model is rather simple, it can fit reasonably well the adsorption of PQ^{2+} , i.e., the

Table 2
Thermodynamic parameters of PQ^{2+} adsorption on TiO_2-SiO_2 .

T (°C)	ΔG° (kJ mol^{-1})	ΔH° (kJ mol^{-1})	ΔS° (J $\text{K}^{-1} \text{ mol}^{-1}$)
15	−3.17	8.45	39.88
25	−3.40		
35	−3.68		
45	−3.99		

Table 3
Best-fit parameters for Eq. (2).

Sample	pH	T (°C)	I (M)	Freundlich isotherm		
				K_F	n	r^2
SiO_2	9.5	25	0	0.08	1.43	0.922
TiO_2-SiO_2	4.4	25	0	1.44	2.18	0.997
TiO_2-SiO_2	7.0	25	0	2.77	2.13	0.994
TiO_2-SiO_2	9.5	25	0	9.10	2.31	0.991
TiO_2-SiO_2	9.5	15	0	9.03	2.33	0.988
TiO_2-SiO_2	9.5	35	0	9.53	2.24	0.987
TiO_2-SiO_2	9.5	45	0	9.61	2.23	0.990
TiO_2-SiO_2	9.5	25	0.01	8.87	2.54	0.999
TiO_2-SiO_2	9.5	25	0.03	7.20	2.60	0.998
TiO_2-SiO_2	9.5	25	0.1	4.98	2.83	0.982

goodness-of-fit of Eq. (2) was checked through the r^2 values, which was between 0.982 and 0.997 in almost all cases.

Changes in pH and ionic strength result in important changes in the adsorption isotherm, i.e., K_F increases as pH increases or ionic strength decreases. On the other hand, slightly changes in these parameters were obtained by changing the temperature from 5 to 45 °C. The Freundlich parameters also show that the adsorption conditions in all cases are favorable ($n > 1$).

4. Conclusions

The results shown in this article reveal that the adsorption of PQ^{2+} is low and only detectable at pH 9.5 on the bare silica surface, and negligible in all experimental conditions on non-supported titania. The neutral framework of SiO_2 and the low surface area of the TiO_2 particle agglomerates seem to be the main factors that prevent the attachment of this herbicide. However, the presence of TiO_2 on the silica surface strongly enhances the adsorption capacity to PQ^{2+} .

The adsorption of PQ^{2+} on TiO_2 – SiO_2 is fast and it takes place by direct binding of the herbicide to the dispersed TiO_2 nanocrystallites and thus ternary surface species of the type SiO_2 – TiO_2 – PQ^{2+} are formed. The adsorption process is mainly electrostatic interactions and/or the formation of charge-transfer or outer-sphere complexes between negatively charged groups of titania and PQ^{2+} , as deduced from adsorption experiments performed at different ionic strengths and temperatures. The analysis of thermodynamic parameters suggests that the adsorption on TiO_2 – SiO_2 is endothermic and spontaneous in nature.

The obtained results have a significant importance in environmental processes. Mesoporous silica is known to be a very good material for several uses (catalyst support, drug delivery, biosensing applications, biochemical separation, etc.) due to its high surface area and pore size. However, since SiO_2 could be modified by the incorporation of metal ions or metal oxides on the mesopore structure, the M – SiO_2 and/or MO_x – SiO_2 (M = metal) systems may act as excellent adsorbents for herbicide control. This will not only benefit the deactivation of herbicides but also reduce their leaching and transport through groundwaters.

Acknowledgments

This work was financed by SECyT-UNS, CONICET and ANPCYT. The authors thank Olga Pieroni and Graciela Mas for the IR spectra and X-ray diffractograms, respectively. M. Brigante thanks CONICET for the postdoctoral fellowship.

References

- [1] S.H. Kim, H.H. Ngo, H.K. Shon, S. Vigneswaran, Sep. Purif. Technol. 58 (2008) 335.
- [2] R.H. Bromilow, Pest Manage. Sci. 60 (2004) 340.
- [3] C.M. Chen, A.C. Lua, J. Toxicol. Environ. Health A 59 (2000) 477.
- [4] R.J. Dinis-Oliveira, F. Remião, H. Carmo, J.A. Duarte, A. Sanchez Navarro, M.L. Bastos, F. Carvalho, Neurotoxicology 27 (2006) 1110.
- [5] J.M. Kleijn, E. Rouwendal, H.P. van Leeuwen, J. Lyklema, J. Photochem. Photobiol., A 44 (1988) 29.
- [6] L. Clausen, I. Fabricius, J. Environ. Qual. 30 (2001) 858.
- [7] M.N. Jones, N.D. Bryan, Adv. Colloid Interface Sci. 78 (1980) 1.
- [8] Y. Seki, K. Yurdakoç, J. Colloid Interface Sci. 287 (2005) 1.
- [9] W.T. Tsai, C.W. Lai, J. Hazard. Mater. B 134 (2006) 144.
- [10] T. Nakamura, N. Kawasaki, H. Ogawa, S. Tanada, M. Kogirima, M. Imaki, Toxicol. Environ. Chem. 70 (1999) 275.
- [11] A. Iglesias, R. López, D. Gondar, J. Antelo, S. Fiol, F. Arce, Chemosphere 76 (2009) 107.
- [12] M. Brigante, G. Zanini, M. Avena, J. Hazard. Mater. 184 (2010) 241.
- [13] C.T. Kresge, M.E. Leonowicz, W.J. Roth, J.C. Vartuli, J.S. Breck, Nature 359 (1992) 710.
- [14] V. Meynen, P. Cool, E.F. Vansant, Microporous Mesoporous Mater. 125 (2009) 170.
- [15] Z.A. AlOthman, A.W. Apblett, Appl. Surf. Sci. 256 (2010) 3573.
- [16] J. Xu, W. Chu, S. Luo, J. Mol. Catal. A: Chem. 256 (2006) 48.
- [17] M. Stöcker, Microporous Mesoporous Mater. 82 (2005) 257.
- [18] B.K. Vu, E.W. Shin, O. Snisarenko, W.S. Jeong, H.S. Lee, Korean J. Chem. Eng. 27 (2010) 116.
- [19] V. Belessi, D. Lambropoulos, I. Konstantinou, R. Zboril, J. Tucek, D. Jancik, T. Albanis, D. Petridis, Appl. Catal., B 87 (2009) 181.
- [20] G. Liu, Z. Chen, C. Dong, Y. Zhao, F. Li, G.Q. Lu, H.M. Cheng, J. Phys. Chem. B 110 (2006) 20823.
- [21] G. Liu, X. Wang, L. Wang, Z. Chen, F. Li, G.Q. Lu, H.M. Cheng, J. Colloid Interface Sci. 334 (2009) 171.
- [22] P.V. Messina, M.A. Morini, M.B. Sierra, P.C. Schulz, J. Colloid Interface Sci. 300 (2006) 270.
- [23] G.P. Zanini, C. Maneiro, Waiman, J.A. Galantini, R.A. Rosell, Geoderma 149 (2009) 110.
- [24] A. Khenifi, Z. Derriche, C. Mousty, V. Prévot, C. Forano, Appl. Clay Sci. 47 (2010) 362.
- [25] M.V. Phanikrishna Sharma, V. Durga Kumari, M. Subrahmanyam, J. Hazard. Mater. 175 (2010) 1101.
- [26] G. Gu, P.P. Ong, C. Chu, J. Phys. Chem. Solids 60 (1999) 943.
- [27] C. He, B. Tian, J. Zhang, Microporous Mesoporous Mater. 126 (2009) 50.
- [28] S.R. Yoganarasimhan, C.N.R. Rao, Trans. Faraday Soc. 58 (1962) 1579.
- [29] J. Yang, J. Zhang, L. Zhu, S. Chen, Y. Zhang, Y. Tang, Y. Zhua, Y. Li, J. Hazard. Mater. B137 (2006) 952.
- [30] Q. Zhang, L. Gao, Langmuir 19 (2003) 967.
- [31] H.P. Klug, L.E. Alexander, X-ray Diffraction Procedures, Wiley, New York, 1954.
- [32] F. Radjy, E.J. Sellevold, J. Colloid Interface Sci. 39 (1972) 367.
- [33] C.E. Zubieta, P.V. Messina, C. Luengo, M. Dennehy, O. Pieroni, P.C. Schulz, J. Hazard. Mater. 152 (2008) 765.
- [34] D.M. Antonelli, J.Y. Ying, Angew. Chem., Int. Ed. Engl. 34 (1995) 2014.
- [35] A.M. Busuioc-Tomoiagă, M. Mertens, P. Cool, N. Bilba, E.F. Vansant, Stud. Surf. Sci. Catal. 74 (2008) 377.
- [36] X. Zhang, F. Zhang, K.Y. Chan, Appl. Catal., A 284 (2005) 193.
- [37] K. Gude, V.M. Gun'ko, J.P. Blitz, Colloids Surf., A 325 (2008) 17.
- [38] V. Zelenák, V. Hornebecq, S. Mornet, O. Schäf, P. Llewellyn, Chem. Mater. 18 (2006) 3184.
- [39] R.J. Davies, Z. Liu, Chem. Mater. 9 (1997) 2311.
- [40] X. Gao, I.E. Wachs, Catal. Today 51 (1999) 233.
- [41] Marek Kosmulski, J. Colloid Interface Sci. 298 (2006) 730.
- [42] V.M. Gun'ko, V.I. Zarko, I.F. Mironyuk, E.V. Goncharuk, N.V. Guzenko, M.V. Borysenko, P.P. Gorbik, O.A. Mishchuk, W. Janusz, R. Leboda, J. Skubiszewska-Zięba, W. Grzegorzczak, M. Matysek, S. Chibowski, Colloids Surf., A 240 (2004) 9.
- [43] H. Zhang, X. Quan, S. Chen, H. Zhao, Environ. Sci. Technol. 40 (2006) 6104.
- [44] H.H. Choi, J. Park, R.K. Singh, Appl. Surf. Sci. 240 (2005) 7.
- [45] J.W. Lee, S. Kong, W.S. Kim, J. Kim, Mater. Chem. Phys. 106 (2007) 39.
- [46] W.T. Tsai, K.J. Hsien, Y.M. Chang, C.C. Lo, Bioresour. Technol. 96 (2005) 657.
- [47] G. Rytwo, S. Nir, L. Margulies, Soil Sci. Soc. Am. J. 60 (1996) 601.
- [48] I.G. Burns, M.B.H. Hayes, M. Stacey, Pest Sci. 4 (1973) 629.
- [49] R. Prada Silvy, F. Lopez, Y. Romero, E. Reyes, V. León, R. Galiasso, Stud. Surf. Sci. Catal. 91 (1995) 281.
- [50] P.V. Messina, P.C. Schulz, J. Colloid Interface Sci. 299 (2006) 305.
- [51] Z.B. Mulu, K. Yurdakoç, Microporous Mesoporous Mater. 127 (2010) 50.
- [52] N. Senesi, V. D'Orazio, T. Miano, Geoderma 66 (1995) 273.
- [53] W. Zou, J. Zhang, F. Chen, Mater. Lett. 64 (2010) 1710.
- [54] E. Tanis, K. Hanna, E. Emmanuel, Colloids Surf., A 327 (2008) 57.